

## Air entrapment effects on infiltration rate and flow instability

Zhi Wang and Jan Feyen

Institute for Land and Water Management, Katholieke Universiteit Leuven, Leuven, Belgium

Martinus Th. van Genuchten

U.S. Salinity Laboratory, USDA-ARS, Riverside, California

Donald R. Nielsen

Department of Land, Air, and Water Resources, University of California, Davis

**Abstract.** Experiments were conducted to quantify the effects of entrapped air on water infiltration into a loamy sand. Transparent three-dimensional (3-D) and 2-D columns were used for experiments carried out for two infiltration conditions: (1) when air was free to move ahead of the wetting front and leave the bottom of the column (air draining) and (2) when air was confined ahead of the wetting front and hence could escape only through the soil surface (air confining). The measurement setup was composed of a tension-pressure infiltrometer, an air flowmeter, water manometers, and video-picture cameras. We applied both positive and negative water pressures at the soil surface and measured the simultaneous changes in the rates of water inflow and air outflow, the air pressure ahead of the wetting front, and the dynamic behavior and advance of the wetting front. The air pressure ahead of the wetting front for the air-confining condition was generally found to increase with time rather than reaching a constant level, as observed in other studies by other researchers. The air pressure fluctuated locally because of air escaping from the soil surface. On the basis of an analysis of the results we present two empirical equations to predict the maximum air pressure at which air begins to erupt from the soil surface and to predict the minimum air pressure at which air eruption stops. We found that the infiltration rate was always equal to, and controlled by, the rate of air outflow. The infiltration rate varied inversely with the air pressure ahead of the wetting front and with the ponding depth at the soil surface. The infiltration rate fluctuated with time rather than undergoing changes in a three-stage process, as is often characterized in the literature. The volume of residual entrapped air in the air-confining condition increased 7% on average, and the infiltration rate decreased threefold to tenfold as compared to the air-draining condition. Finally, it was shown that the air-confining infiltration flow is fingered and unstable, consistent with the predictions of an existing theory.

### 1. Introduction

The movement of water into and through the vadose zone is in essence a problem of immiscible displacement between air and water in a porous medium. As water infiltrates into the vadose zone, soil air is being displaced and may become compressed ahead of the wetting front. Existing laboratory studies [Wilson and Luthin, 1963; Peck, 1965; Adrian and Franzini, 1966; Latifi *et al.*, 1994] and field experiments [Bodman, 1937; Dixon and Linden, 1972; Jalali-Farahani *et al.*, 1993] have shown that soil air compression can lead to a substantial decrease in the rate of infiltration. When the air pressure is sufficiently high, air will escape from the soil surface, thereby causing a sharp decrease in air pressure and a major increase in the rate of water infiltration [McWhorter, 1971; Vachaud *et al.*, 1974; Touma *et al.*, 1984; Grismer *et al.*, 1994]. Air compression below the wetting front will generally also lead to residual air entrapment in the transmission zone [Vachaud *et al.*, 1974; Touma *et al.*, 1984]. An uneven distribution of air

pressure in the subsurface can cause the shallow groundwater table to decrease or increase locally [Linden and Dixon, 1973]. During periods of intense rainfall, compressed soil air may break upward through the soil surface, thereby often lifting and detaching soil particles, leading to increased runoff and erosion [Jarrett and Fritton, 1978; Suhr *et al.*, 1984].

Although several attempts have been made to mathematically simulate the complex effects of air entrapment on infiltration properties [Morel-Seytoux and Khanji, 1974; Morel-Seytoux and Billica, 1985; Parlange and Hill, 1979; Sander *et al.*, 1988], the underlying physical processes affecting infiltration in the presence of entrapped air are still not fully understood conceptually. Also, testing of available theoretical approaches is seriously hampered by a lack of experimental studies of the underlying processes. The present study attempts to quantify the effect of air entrapment on infiltration through a series of experiments using a dry sand. An experimental setup was designed to measure simultaneous changes in air pressure ahead of the wetting front, the rate of water inflow, the rate of air outflow, and the dynamic advance of the wetting front. We applied both constant (ponded) and variable (suction) pressure heads at the soil surface. The effects of entrapped air on

Copyright 1998 by the American Geophysical Union.

Paper number 97WR02804.  
0043-1397/98/97WR-02804\$09.00

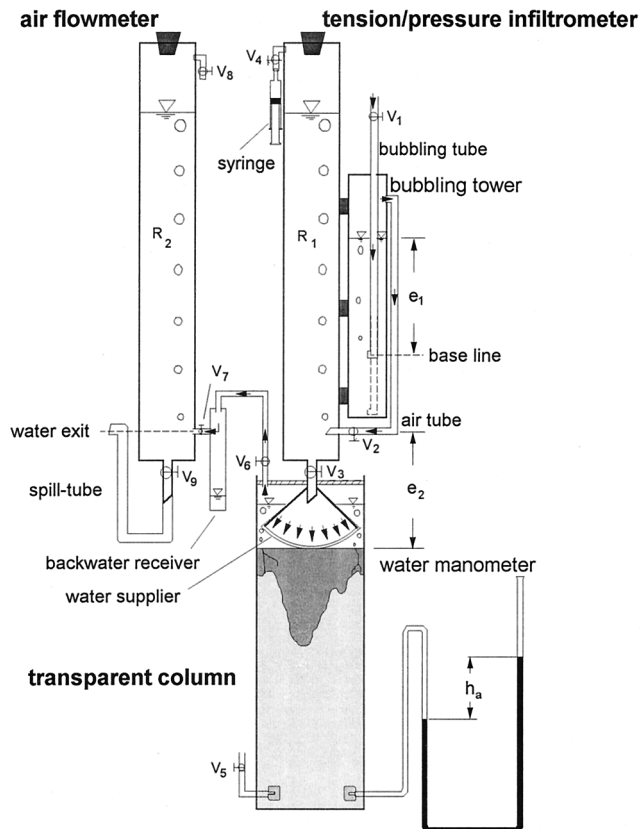


**Figure 1.** Experimental setup for simulating the effects of air entrapment on infiltration.  $V$  denotes valves used to refill the water reservoirs ( $R_1$  and  $R_2$ ) and to control air release from the soil column.

the hydraulic conductivity and on the onset and extent of unstable flow (fingering) are also assessed.

## 2. Experimental Approach and Materials

The laboratory setup was composed of a soil column, a tension-pressure infiltrometer, and an air flowmeter (Figure 1). A three-dimensional (3-D) column (cylinder inner diameter of 8.6 cm and soil height of 45 cm) was constructed of transparent polyvinyl chloride, and a 2-D column (41.5 cm wide, 2.8 cm thick, and with a 50-cm sample height) was constructed of 1-cm-thick transparent acrylic plastic. Both columns were open at the top and closed at the bottom and sides. Air-confining conditions were achieved by closing the bottom valve  $V_5$  (Figure 1), and air-draining conditions were achieved by opening the valve. The soil air pressure was measured 10, 20, 30, and 45 cm below the soil surface using water manometers (ID = 3 mm). Porous air transmission stones were connected to the inlet end of each manometer.

We used a modified tension (disc) infiltrometer [Perroux and White, 1988] to apply both positive pressure heads (ponding) and suctions (nonponding conditions) at the soil surface. The traditionally installed disc was replaced in our setup (Figure 1) with a convex-shaped water supplier to allow air to escape from the soil surface. Also, the bubbling tube was allowed to move up and down in the vertical direction. As shown in Figure 1, the water pressure at the bottom of the water supplier (the infiltration surface) could be regulated by adjusting the height  $e_1$

of the water level in the bubbling tower relative to  $e_2$ , the vertical distance between the air tube and the water supplier. When the bubbling tube is set at the baseline defined by  $e_1 = e_2$ , the pressure at the infiltration surface will be zero. When  $e_1 < e_2$ , a positive pressure head (ponding) will result, whereas when  $e_1 > e_2$ , a negative pressure head (suction) will be imposed at the infiltration surface. When supplying a zero or negative pressure head at the soil surface, the convex base was flattened to the soil surface to ensure good contact; however, a 5-mm gap was always maintained between the flattened water supplier and the column walls to enable the escape of air from the surface. With such a tension infiltrometer it is also possible to measure the dynamic air-bubbling (air entry) and water-bubbling (water entry) values of a porous medium (see detailed descriptions by Fallow and Elrick [1996]). During our measurements of the water and air entry values the water supplier was always completely buried in the sand (instead of being placed on the surface) to ensure good contact between the soil matrix and the water supplier.

The air flowmeter consisted of a Marriotte reservoir  $R_2$  and a spill tube, which discharged water as air entered the reservoir  $R_2$ . The water exit of the spill tube was set at the same level as the air inlet tube (with valve  $V_7$ ). A backwater receiver was placed between the air transmission tube (with valve  $V_6$ ) and the air flowmeter to receive any possible reverse flow from reservoir  $R_2$ . This situation will occur when the water level on the soil surface decreases, thereby creating a vacuum condition in the headspace of the soil column. At the end of infiltration under air-draining conditions, air bubbles may be leaving the bottom of soil columns, together with water. The volumes of mixed air and water could be separated and measured using the air flowmeter. The air bubbles would move upward into the headspace of reservoir  $R_2$ , while the water would leave the system immediately through the water exit.

Washed, oven-dried sand (4.5% clay, 11.3% silt, and 84.2% sand) was poured into the transparent 3-D column using a funnel tube with inside wire screens to randomize the falling sand. The sand was initially consolidated by first dropping the sample 200 times from an elevation of 5 cm and subsequently using a vibrator. The top few centimeters of the sand were removed to eliminate nonuniformities in bulk density near the soil surface. The final soil height of the packed samples was 45 cm, and the average bulk density was  $1.60 \pm 0.02 \text{ g cm}^{-3}$ . Assuming a particle density of  $2.65 \text{ g cm}^{-3}$ , the total porosity  $\phi = 0.40 \pm 0.02$ . The same packing method was used for the 2-D column. Several experiments using a constant head permeameter [Klute and Dirksen, 1986] indicated that the natural saturated hydraulic conductivity  $K_s$  of the sand was  $2217 \text{ cm d}^{-1}$  ( $2.57 \times 10^{-4} \text{ m s}^{-1}$  or  $15.4 \text{ mm min}^{-1}$ ). Air-confining infiltration tests under constant water heads of  $-10, -5, 0, 3, 5, 6, 8,$  and  $10 \text{ cm}$  and under variable water heads from  $-10$  to  $0 \text{ cm}$ ,  $0$  to  $3 \text{ cm}$ , and  $0$  to  $10 \text{ cm}$  were conducted. Each experiment was repeated, and the results were compared with those from the air-draining tests. We used distilled water for all experiments. A video camera (SONY model CCD-TR808E) was used to record the development of wetting fronts in the soil column, the falling water levels in reservoirs  $R_1$  and  $R_2$ , and air pressure heads, as indicated in the water manometers. Images of the wetting front advancement were later digitized into computer plot files using the ARC/INFO and AutoCAD hardware and software packages.

### 3. Experimental Results and Discussion

#### 3.1. Air Compression Ahead of the Wetting Front

Dynamic changes in air pressure 10, 20, 30, and 45 cm below the soil surface were measured as water infiltrated into the sand. Our purpose was to examine the magnitude and distribution of air pressures ahead of the wetting front. Results are shown in Figure 2.

In the air-draining dry sand column (Figure 2a) the soil air pressure  $h_a$ , in excess of the atmospheric pressure, was small and relatively uniform at all levels ahead of the wetting front. The value of  $h_a$  varied between 2 and 4 cm of water. A sharp wetting front was present, as indicated by very similar values of the maximum,  $Z_{max}$ , and the minimum,  $Z_{min}$ , wetting depths. When the wetting front reached the bottom of the column, after  $\sim 8$  min,  $h_a$  at all levels increased significantly owing to water intrusion into the manometers.

In the air-confining dry column (Figure 2b), air pressures ahead of the wetting front initially rose uniformly to a high of  $\sim 20$  cm at  $t = 2$  min. At about  $t = 7$  min and  $t = 38$  min, soil air started to erupt from the top, which in turn led to immediate decreases in  $h_a$ . After  $t = 9$  min the infiltrating water submerged the highest air pressure sensor at  $z = 10$  cm, which caused the value of  $h_a$  at this depth to remain at about  $h_a = 14$  cm. The air pressure below the wetting front uniformly increased to  $h_a > 40$  cm. Following the third air eruption at  $t = 38$  min,  $h_a$  rose very abruptly to a maximum value of 47 cm at  $t = 55$  min. The wetting front was deformed from the very beginning of infiltration, with a wetting tip (given by  $Z_{max}$ ) occupying about half of the circumference of the column wall and moving much more rapidly than the wetting tail (given by  $Z_{min}$ ).

In the air-draining prewetted column (Figure 2c) the sample was drier at the top but saturated at the bottom. Immediately upon infiltration, the soil air pressure  $h_a$  increased at the upper locations in the column (10, 20, and 30 cm); however, the bottom air pressure at  $z = 45$  cm remained zero. Water at the bottom of the column impeded the air flow. The air pressure difference between the saturated top layer and the "water table" at the bottom caused water to flow out of the bottom of the column. The air pressure at 10 cm remained at relatively low values (between 10 and 14 cm) owing to submergence of the air pressure sensor at this level. Air pressures in the middle of the column (20–30 cm below the soil surface) generally increased simultaneously to a maximum of 30 cm, except for temporary decreases at  $t = 0.2, 2,$  and  $5$  min when air bubbles erupted from the top.

As previously noted by Fayer and Hillel [1986], air entrapment can be an important factor in lysimeter studies of infiltration. For example, following the addition of water or a solute solution to the surface, the air pressure inside the lysimeter may increase, resulting in a near-immediate water discharge from the bottom. The amount of water being then discharged could be misinterpreted as fluid breakthrough from the applied water, or a decrease in the water table could be misinterpreted as direct evaporation from the soil surface.

#### 3.2. Rates of Water Inflow and Air Outflow Under Constant and Variable Pressure Heads

Air-draining infiltration under a nonponding constant head  $h_0$  of  $-10$  cm (Figure 3a) resulted in a constant infiltration rate  $i_w$ , which was lower than the saturated hydraulic conductivity  $K_s$  ( $15.4 \text{ mm min}^{-1}$ ) of the sand. The air outflow rate  $i_a$  from

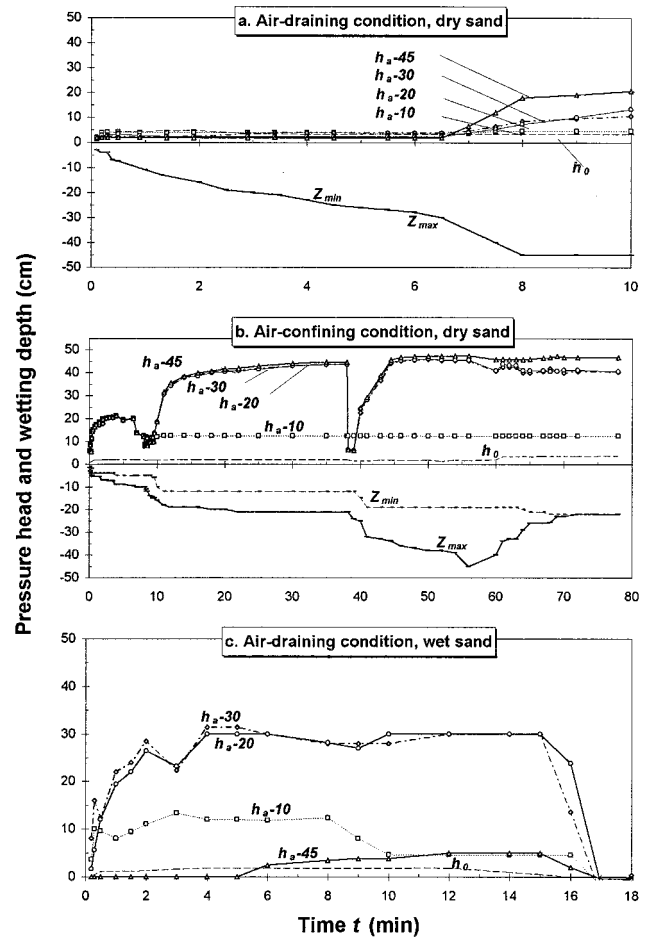


**Figure 2.** Air pressure variation with time in (a) an air-draining dry sand column, (b) an air-confining dry sand column, and (c) an air-draining prewetted sand column. The gage air pressure  $h_a$  was measured at depths of 10, 20, 30, and 45 cm below the soil surface as shown by the  $h_a-10$  (squares),  $h_a-20$  (circles),  $h_a-30$  (diamonds), and  $h_a-45$  (triangles) data points, respectively.  $Z_{max}$  and  $Z_{min}$  are the maximum and minimum wetting depths, respectively, and  $h_0$  is the ponding depth on the soil surface.

the bottom of the column was equal to the water inflow rate  $i_w$ . The soil air pressure  $h_a$  remained constant and close to zero. When the soil surface was saturated at  $h_0 = 0$  cm (Figure 3b) at  $z = -45$  cm (bottom of the column) and  $h_0 = 10$  cm (Figure 3c),  $i_w$  and  $i_a$  were initially much greater than  $K_s$  but then slowly approached  $K_s$ . The soil air pressure remained close to zero during most of the infiltration period. The abrupt increase in air pressure at the end of infiltration was caused by water entry into the water manometer. With air draining from the bottom the rate of infiltration monotonically increased, and the total time of infiltration decreased with the increase in  $h_0$ .

Results of the air-confining experiments under constant surface pressure heads are shown in Figure 4, where  $i_a$  now indicates the rate of air outflow from the soil surface. When a negative pressure head  $h_0$  of  $-10$  cm (Figure 4a) was imposed, both the water inflow rate  $i_w$  and the air outflow rate  $i_a$  initially increased simultaneously. The air pressure  $h_a$  then remained equal to zero. After 2 min,  $h_a$  increased sharply to 10 cm at  $t = 4$  min, whereas  $i_w$  and  $i_a$  decreased abruptly. During the remaining period of infiltration, with  $h_a$  monotonically increas-

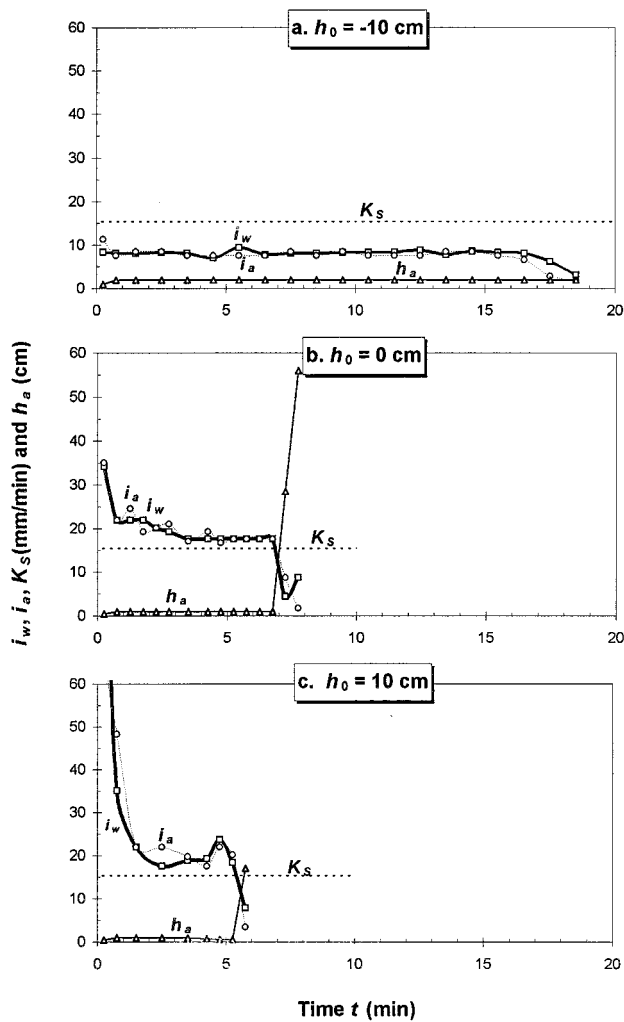


**Figure 3.** Water inflow rate  $i_w$  (squares), air outflow rate  $i_a$  (circles), and gage air pressure ahead of the wetting front  $h_a$  (triangles) as functions of time  $t$  for the air-draining condition under (a) a negative constant pressure source, (b) a constant zero head, and (c) a constant ponding head.

ing with time at a slower pace,  $i_w$  and  $i_a$  remained at a low level and were equal to each other. Under a zero water head ( $h_0 = 0$ , Figure 4b) both  $i_w$  and  $i_a$  decreased simultaneously to a minimum value when  $h_a$  increased continuously upon infiltration. These results indicate that the soil surface was quickly sealed by water at the surface, leading to immediate compression of air below the wetting front. After air eruption from the soil surface at about  $t = 2$  min,  $i_a$  and  $i_w$  increased, while  $h_a$  decreased sharply. After 4 min,  $h_a$  started to increase steadily, whereas  $i_a$  and  $i_w$  decreased again toward zero. The variation in  $i_w$  in this case closely resembled the three-phase infiltration pattern, as described by Christiansen [1944], McWhorter [1971], and Vachaud *et al.* [1974]. Christiansen suggested that the second increase in  $i_w$  was caused by the gradual dissolution of entrapped air into the water. However, the results by McWhorter [1971] and Vachaud *et al.* [1973, 1974], as well as our experiments, indicate that eruption of compressed air from the soil surface was the main reason for the increase in  $i_w$ . For the ponded condition  $h_0 = 10$  cm (Figure 4c),  $i_w$  initially decreased, while  $i_a$  increased starting from zero. After the initial

air escape from the soil surface,  $i_a$  and  $i_w$  became identical and remained relatively small.

The air-confining experimental results revealed pronounced increases in air pressure  $h_a$  with increasing  $h_0$ . The maximum  $h_a$  attained under the negative pressure head ( $h_0 = -10$  cm, Figure 4a) was 32 cm of water. Under zero pressure (Figure 4b),  $h_a$  reached a maximum of 46 cm, while for ponding ( $h_0 = 10$  cm, Figure 4c)  $h_a$  increased to 49 cm. Contrary to the results obtained for the air-draining condition (Figure 3),  $i_w$  did not monotonically increase with  $h_0$ , nor did  $i_w$  always decrease with time. The value of  $i_w$  appeared to vary inversely with air pressure  $h_a$ . Notice that the highest imposed surface pressure (Figure 4c) resulted in the lowest infiltration rate. Hence water infiltration into an air-confined medium is negatively affected by the ponding depth on the surface. With air compression ahead of the wetting front (Figure 4) both  $i_w$  and  $i_a$  were reduced to values much lower than those for the air-draining condition (Figure 3). For the nonponding condition ( $h_0 = -10$  cm) the time needed to wet the entire sand column increased almost 4 times, from 18 min (as shown in Figure 3a) to 70 min (Figure 4a). For the ponding condition

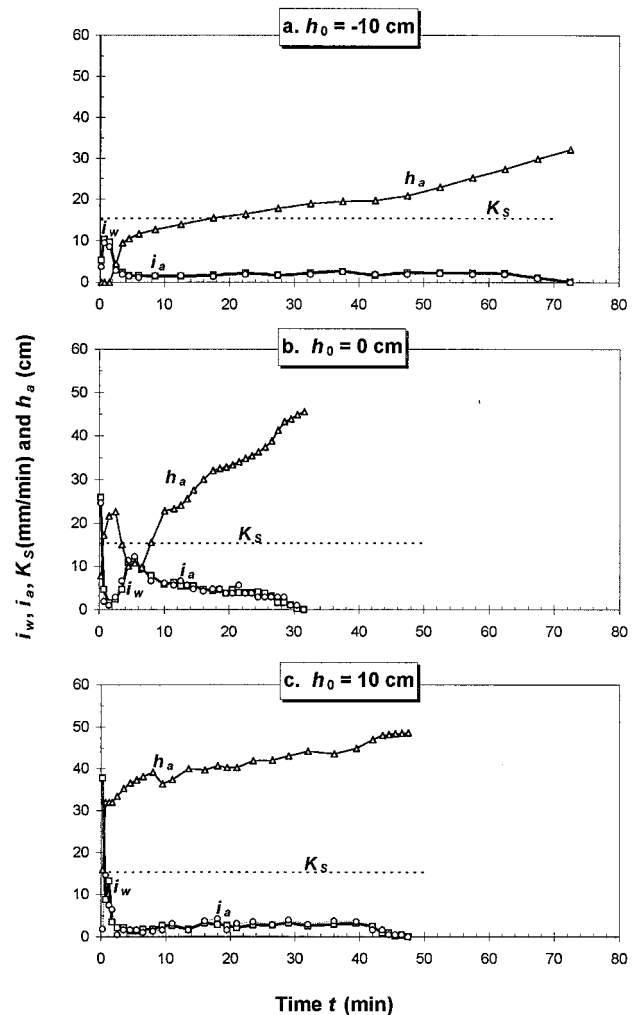


**Figure 4.** Water inflow rate  $i_w$  (squares), air outflow rate  $i_a$  (circles), and gage air pressure ahead of the wetting front  $h_a$  (triangles) as functions of time  $t$  for the air-confining condition under (a) a negative constant pressure head, (b) a constant zero head, and (c) a constant ponding head.



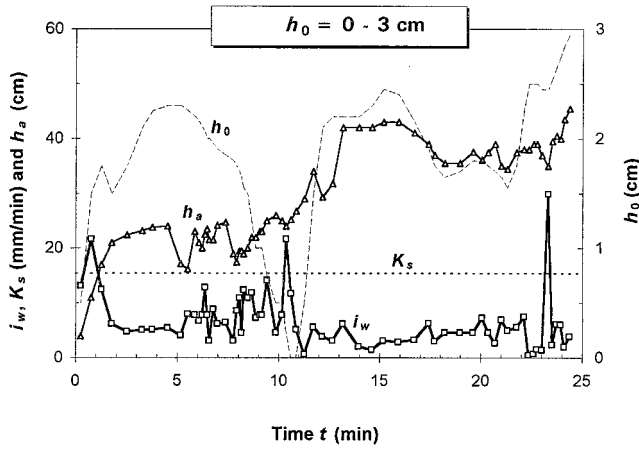


**Figure 5.** Water inflow rate  $i_w$  (squares) and gage air pressure ahead of the wetting front  $h_a$  (triangles) as functions of time  $t$  for the air-confining condition under the ponded variable pressure head  $h_0 = 0 \sim 3$  cm.

( $h_0 = 10$  cm) the required wetting time increased 10 times, from 5 min in Figure 3c to 48 min in Figure 4c.

Our experiments for a variable surface water head under air-draining conditions produced almost the same values for the air pressure and infiltration rate as those obtained with the constant head experiment (Figure 3), and thus are not further reported here. However, the varying ponded pressure head experiment resulted in more abrupt variations in air pressure  $h_a$  and the infiltration rate  $i_w$ . As shown in Figure 5, a slight decrease in  $h_0$  and  $h_a$  sometimes triggered substantial jumps in  $i_w$ . The jump in  $i_w$  was especially pronounced when the air pressure below the wetting front became relatively high (e.g., at  $t = 23$  min). Similar increases in infiltration rate were also noted in several field plots submerged for long periods of time [Bodman, 1937; Christiansen, 1944]. A decrease in  $h_0$  may have suddenly reversed the direction of interfacial air-water displacement (i.e., from a downward displacement of air by water to an upward displacement of water by air). As a result, the highly pressurized air suddenly breaks through the soil surface, thereby causing a major jump in  $i_w$ . We observed that during the escape of air bubbles, sand particles also erupted from the soil surface. The air and sand eruptions created small openings or holes (2–5 mm in diameter) in the sand surface; this caused the top layer to become much more loose than the undisturbed sublayer. Air eruption holes are often observed on sea beaches at the moment when a sea wave recedes.

We found from the inflow-outflow data that the volumes of

**Table 2.** Comparison of the Average Water Infiltration Rate  $i_w$  in the Air-Confining and Air-Draining Columns

Surface Water Head $h_0$ , cm	Air-Confining Condition		Air-Draining Condition	
	Infiltration Rate $i_w$ , mm min <sup>-1</sup>	Saturated Conductivity $K_s$ , %	Infiltration Rate $i_w$ , mm min <sup>-1</sup>	Saturated Conductivity $K_s$ , %
-10	8	52	2	13
-5	9	58	3.5	23
0	19	123	4	26
3	20	130	5	32
5	20	130	2	13
10	20	130	2	13

water inflow and air outflow for the air-draining condition both were much greater than the volumes for the air-confining condition (Table 1). This result reflects the greater volume of entrapped air in the air-confining columns. The average residual air saturation  $S_{nw,0}$  in the air-draining columns was  $\sim 20\%$ , which is comparable to the 19% obtained by Vachaud *et al.* [1974] and the 15.6% obtained by Touma *et al.* [1984]. Residual air saturation  $S_{nw,c}$  in the air-confining condition was 27.3% on average, very similar to the 23.8% obtained by Vachaud *et al.* [1974] and the 26.5% obtained by Touma *et al.* [1984]. The data indicate that  $S_{nw,c}$  is  $\sim 7\%$  higher than  $S_{nw,0}$ . Owing to the increase in residual air, the hydraulic conductivity in the wetted region is reduced. The natural saturated water content for the air-draining condition can be estimated as  $\theta_s = \phi(1 - S_{nw,0}) = 0.4(1 - 0.176) = 0.33$ . For the air-confining condition the average water content in the wetted zone was  $\theta_w = \phi(1 - S_{nw,c}) = 0.278$ , corresponding to an effective water content of  $\theta^* = \theta_w \theta_s^{-1} = 0.842$ . The van Genuchten [1980] estimate ( $m = 1 - n^{-1}$ , Table 3) of the relative hydraulic conductivity  $k_{rw}$  in the transmission zone results in  $k_{rw} = \theta^{*1/2}[1 - (1 - \theta^{*1/m})m]^2 \equiv 0.4$ . This indicates that the hydraulic conductivity during the air-confining condition is reduced by 60% as compared to the air-draining condition.

The water pressure gradient across the transmission zone also decreased due to the fact that the soil air pressure balances the capillary suction at the wetting front [Grismer *et al.*, 1994]. Decreases in both the hydraulic conductivity and the pressure gradient combine to reduce the infiltration rate. The data in Table 2 indicate the average water inflow rate  $i_w$  for the air-draining condition was 3–10 times that for the air-confining condition. Under the nonponding condition ( $h_0 < 0$ ),  $i_w$  decreased on average from 55% of the saturated conductivity  $K_s$  for the air-draining condition to 18% of  $K_s$  for the air-

**Table 1.** Comparison of Residual Air Entrapment Following Infiltration Into Air-Draining and Air-Confining 3-D Columns

Surface Water Head $h_0$ , cm	Air-Draining Columns				Air-Confining Columns			
	Water Inflow, cm <sup>3</sup>	Air Outflow, cm <sup>3</sup>	Entrapped Air, cm <sup>3</sup>	Residual $S_{nw,0}$ , %	Water Inflow, cm <sup>3</sup>	Air Outflow, cm <sup>3</sup>	Entrapped Air, cm <sup>3</sup>	Residual $S_{nw,c}$ , %
-10	867	816	230	22.0	867	788	258	24.6
-5	948	849	197	18.8	874	755	291	27.8
0	892	761	285	27.2	860	805	241	23.0
5	941	862	184	17.6	802	727	319	30.5
10	957	885	161	15.4	815	728	318	30.4
Average				20.2				27.3

Residual air saturation is given as a percentage of the total volume of soil pores (1045 cm<sup>3</sup> corresponding to the total porosity,  $\phi = 0.4$ ).

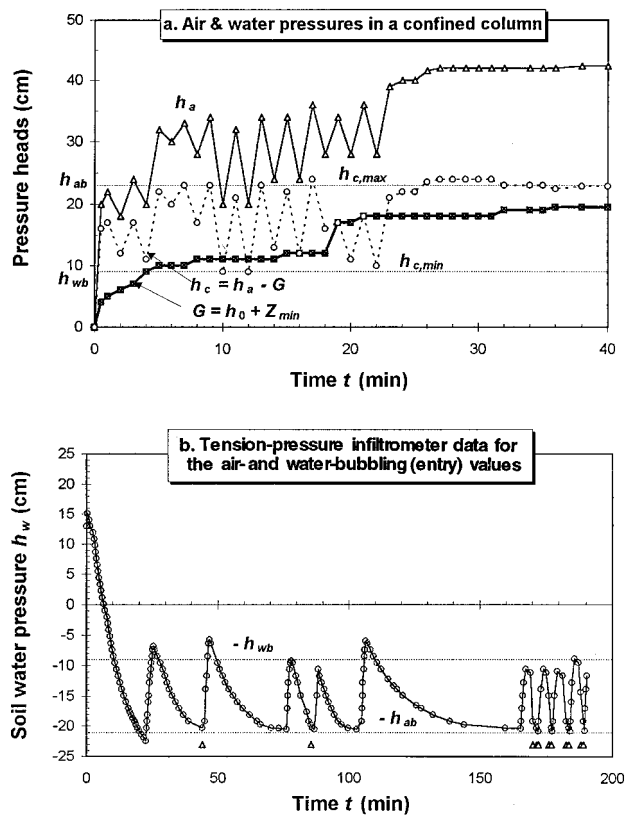


**Figure 6.** Relationships between air pressures, water pressures, and the capillary bubbling (entry) pressures of the sand. (a) Air pressure  $h_a$  (triangles), water pressure  $G = h_0 + Z_{min}$  (solid squares), and the capillary pressure  $h_c = h_a - G$  (circles), as functions of time  $t$  during water infiltration under  $h_0 = 2$  cm into an air-confining column. (b) Tension infiltrometer data show the changes in soil water pressure  $h_w$  (circles). The capillary air-bubbling and water-bubbling pressures  $h_{ab}$  and  $h_{wb}$  correspond to the average minimum and maximum values of  $h_w$  (relative to the atmospheric condition  $h_a = 0$ ), respectively. The triangles in Figure 6b indicate vacuum assistance provided through use of a syringe attached to valve  $V_4$  in Figure 1 to accelerate the measurement.

confining condition. Values of  $i_w$  under the ponded pressure heads ( $h_0 \geq 0$ ) were reduced by a factor of 6, from 128% of  $K_s$  for the air-draining condition to 21% for the air-confining condition. For all pressure heads tested,  $i_w$  decreased from an average of 104% of  $K_s$  for the air-draining condition to an average of 20% of  $K_s$  for the air-confining condition. Constantz *et al.* [1988] previously found from field experiments with air entrapment effects that the hydraulic conductivity of the transmission zone remained less than 20% of the saturated conductivity. Our experiments help to explain the dynamic behavior of infiltration in the field when air entrapment occurs ahead of the wetting front.

We conclude from the foregoing air-confining experiments that the entrapped air pressure in the sand generally increases with time, while fluctuating locally during the entire infiltration period (i.e., not merely being a three-stage process) as a result of intermittent air escape from the soil surface. The rates of water inflow into the soil and air outflow from the soil were approximately equal after air breakthrough from the soil surface. The rates of water inflow into the soil and air outflow from the soil were approximately equal after air breakthrough

from the soil surface. The water inflow and air outflow rates changed inversely with air pressure ahead of the wetting front and with the ponded water depth on the surface. For the foamy sand the average values of  $i_w$  and  $i_a$  were reduced by 70–90% as compared to the air-draining condition. Finally, the results indicate that a minor perturbation in surface water depth may introduce an immediate and abrupt jump in the rates of air outflow and water inflow. The immiscible, intermittent displacement between air and water appears to control the process of water infiltration into the vadose zone.

### 3.3. Air-Breaking and Air-Closing Pressures

Inasmuch as air is compressible the soil air phase should not be neglected when considering air-water immiscible two-phase flow. The counterbalancing effects of water pressure and air pressure at the wetting front control the flux of air and water. Under air-draining conditions the air phase remains close to atmospheric pressure and can escape readily at the same rate as water infiltrates. However, under air-confining conditions, air is compressed by water. When the air pressure becomes sufficiently high, the air phase penetrates into the water phase through large holes created by the air pressure erupting at the saturated top layer.

The maximum air pressure at which air escapes from a ponded surface is referred to here as the “air-breaking value”  $H_b$  (expressed in water height), whereas the minimum pressure at which air eruption stops is called the “air-closing value”  $H_c$ . We observed that air eruption from the surface started and stopped rather suddenly. The flow process was highly dynamic with abrupt increases in the rates of both air outflow and water inflow. However, flow was relatively static beyond the periods of air eruption. Immediately before and after air eruption, the rates of water inflow and air outflow were nearly zero. For an air bubble to escape from a ponded soil surface the entrapped air phase must have a sufficiently high air pressure to overcome the static water pressure,  $G = h_0 + Z_{min}$ , above the entrapped air phase at the wetting front (where  $Z_{min}$  is the minimum wetting depth or the thickness of the saturated top layer). The presence of a saturated top layer had been observed by many researchers in the past; this layer was recently recognized as being a zone for distribution flow from which preferential flow seems to emerge [Ritsema *et al.*, 1993]. The saturated top layer will be slightly desaturated during air eruption through the large air holes. The top layer and air holes become again saturated after air eruption from the top. A typical relationship between the compressed air pressure  $h_a$  and the water head at the wetting front  $G$  is shown in Figure 6a for infiltration under  $h_0 = 2$  cm in an air-confining column. Also plotted in Figure 6a is the capillary pressure at the air-water interface  $h_c$  evaluated as the air pressure in excess of  $G$  (i.e.,  $h_c = h_a - G$ ). The maximum value of  $h_c$ , shown by the peaks of the  $h_c - t$  curve, was nearly constant for a specific column and varied within a narrow range from 22 to 32 cm for all columns. The minimum value of  $h_c$ , shown by the lowest points of the  $h_c - t$  curve, was also nearly constant for a specific column and varied within a narrow range from 5 to 18 cm for all columns. According to Youngs and Peck [1964] this maximum pressure difference  $h_{c,max}$  should be equal to the air-bubbling (air entry) value  $h_{ab}$  of a soil. One may similarly define the water-bubbling (water entry) value  $h_{wb}$  of a soil as the minimum difference  $h_{c,min}$ , which is consistent with the fact that water started to displace air.

Mathematically,  $h_{ab}$  and  $h_{wb}$  are defined as the inflection

points on the main drainage and main wetting retention curves of the soil, respectively. Assuming *van Genuchten's* [1980] model for the soil water retention curve  $S_e(h)$ , the inflection point corresponding to  $d^2h_c/dS_e^2 = 0$  is located at the point  $P(h_c^*, S_w^*)$  with coordinates

$$h_c^* = \frac{1}{\alpha} \left[ \frac{n-1}{n(m+1-n+1)} \right]^{1/n} = \begin{cases} \frac{m^{1/n}}{\alpha} & m = 1 - 1/n \\ \frac{1}{\alpha} & m = 1 - 2/n \end{cases} \quad (1)$$

$$S_e^* = \frac{1}{\alpha} \left[ 1 - \frac{n-1}{m(m+1)} \right]^m = \begin{cases} \left( \frac{1}{1+m} \right)^m & m = 1 - 1/n \\ 0.5^m & m = 1 - 2/n \end{cases} \quad (2)$$

where  $\alpha$ ,  $m$ , and  $n$  are drainage retention parameters and  $S_e$  is the effective saturation. Physically, the air-bubbling value  $h_{ab}$  is the minimum capillary pressure required for air to enter the pore network of an initially water-saturated matrix, whereas the water-bubbling value  $h_{wb}$  is the maximum capillary pressure required for water to penetrate into an initially dry porous matrix [Hillel and Baker, 1988]. Three different forms of *van Genuchten's* [1980] retention model (as shown in Table 3) gave static air-bubbling values of  $h_{ab} \equiv h_c^*$  of 13, 15, and 17 cm, corresponding to effective saturation  $S_e^*$  values of 0.80, 0.74, and 0.69, respectively. As suggested by *Corey and Brooks* [1975] the dynamic effects of moving water and air on the retention curves should be considered when modeling the infiltration process.

The tension-pressure infiltrometer data for the dynamic air-bubbling value  $h_{ab}$  and for the dynamic water-bubbling value  $h_{wb}$  of the sand are shown in Figure 6b. The lowest soil water pressures reflect the dynamic air entry into the initially saturated sand, whereas the highest soil water pressures indicate water entry into the desaturated soil. The soil water pressure at air entry was about  $h_w = -21$  cm of water; this dynamic air-bubbling value should be [Corey and Brooks, 1975, p. 253], "a few centimeters higher than the static result." The dynamic water-bubbling (capillary pressure) value shown in Figure 6b is approximately  $h_{wb} = 9$  cm. Note that this value is only slightly smaller than "one-half of the air-bubbling value," as suggested by *Bouwer* [1966] and *Luckner et al.* [1989].

The average air-bubbling value  $h_{ab}$  and the water-bubbling value  $h_{wb}$  shown in the air-confining infiltration test (Figure 6a) are approximately equal to the values obtained using the tension-pressure infiltrometer method [Fallow and Elrick, 1996], as shown in Figure 6b. During periods of air pressure increases (Figure 6a) or soil water pressure decreases (Figure 6b), air breaks into the wetted layer and the soil water retention curve (SWRC) follows a drainage branch toward desaturation of the wetted layer. On the other hand, during periods when the air pressure decreases (Figure 6a) or the water pressure increases (Figure 6b), the SWRC follows a scanning wetting curve toward resaturation of the sample. We conclude from the above experimental results that fluctuation in the entrapped soil air pressure is a result of hysteresis.

Analysis of our experimental results suggests that the following empirical relationships exist for the air-breaking value  $H_b$  and the air-closing value  $H_c$ :

$$H_b = Z_{\min} + h_0 + h_{ab} \quad (3)$$

**Table 3.** Optimized *van Genuchten* [1980] Drainage Retention Parameters  $\alpha$ ,  $m$ , and  $n$  of the Loamy Sand and the Capillary Pressure  $h_c^*$  and Effective Saturation  $S_e^*$  Corresponding to the Inflection Point on the Drainage Retention Curve

<i>van Genuchten</i> Model Type	$\alpha$ , $\text{cm}^{-1}$	$m$	$n$	$h_c^*$ , cm	$S_e^*$
$m, n$ Variable	0.091	0.158	7.866	12.67	0.80
$m = 1 - 2/n$	0.067	0.441	3.579	14.93	0.74
$m = 1 - 1/n$	0.053	0.705	3.390	17.02	0.69

$$H_c = Z_{\min} + h_0 + h_{wb} \quad (4)$$

As reflected in (3) and (4), the maximum and the minimum entrapped air pressures generally increase when the saturated top layer ( $Z_{\min}$  increases) becomes thicker. At the same time, the air pressures are also subject to changes in the surface water head  $h_0$  and the air- and water-bubbling values  $h_{ab}$  and  $h_{wb}$  of the porous medium. Hence one can predict that if the capillary pressure  $h_c = h_a - (Z_{\min} + h_0)$  at the air-water interface exceeds the air-bubbling value  $h_{ab}$  of the porous medium, air must escape from the soil surface. Conversely, if  $h_c$  becomes less than the water-bubbling value  $h_{wb}$  of the material, the top layer will be resaturated. The thickness of the top layer also increases because the top layer was previously disturbed by the air eruption paths (cracks or channels), which lead to a decrease in the water-bubbling value of the top layer. A lower water-bubbling suction in the top layer allows water to penetrate into the sublayer.

#### 4. Wetting Front Instability and Preferential Flow Induced by Air Compression

Several authors [e.g., Raats, 1973; Philip, 1975; White et al., 1977] previously showed that preferential flow is affected by air compression ahead of the wetting front. During water infiltration into a sand, gravity fingering dominates the effect of capillary forces [Glass et al., 1991]. Neglecting the viscosity and density of air with respect to those of water, the original linear instability criterion [Saffman and Taylor, 1958; Chouke et al., 1959] can be simplified [Parlange and Hill, 1976] to

$$i_w < K_s \quad (5)$$

Thus any time the infiltration rate is less than the saturated hydraulic conductivity of the porous medium the wetting front is predicted to be unstable. Assuming an initial sharp wetting front in the homogeneous sand,  $i_w$  can also be calculated as

$$i_w = K_s \left( 1 - \frac{h_{wf} - h_0}{L} \right) = K_s \left( 1 - \frac{h_{af} - h_{wb} - h_0}{L} \right) \quad (6)$$

where  $h_{wf}$  is the water pressure head immediately above the wetting front,  $h_{af}$  is the gage air pressure immediately below the wetting front,  $h_{wb}$  is the capillary water-bubbling (water entry) pressure of the medium, and  $L$  is the depth of wetting. Substituting (6) into (5), we obtained an alternative criterion for predicting the onset of instability at the wetting front:

$$F = h_0 + h_{wb} - h_{af} < 0 \quad (7)$$

This supplementary criterion is identical to those obtained previously by *Raats* [1973] and *Philip* [1975] using different

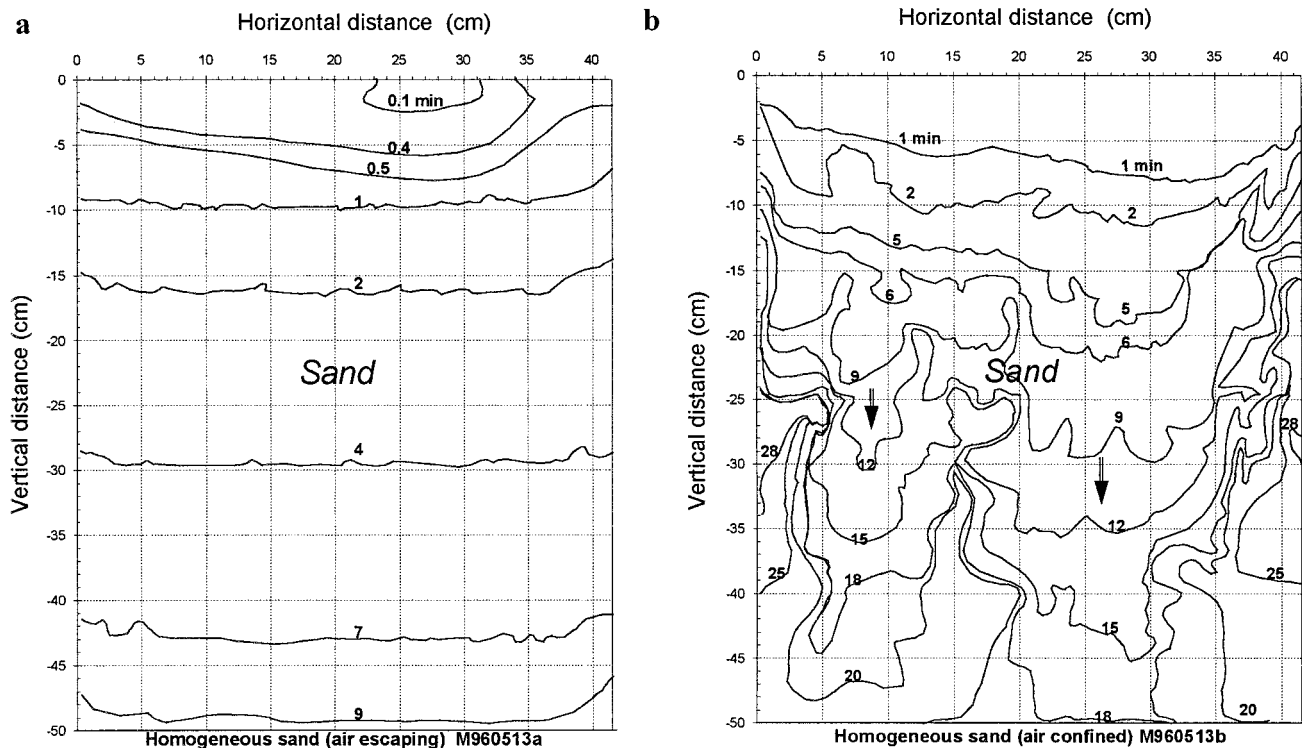


**Figure 7.** Wetting front advancement in the 2-D column (a) stable flow for the air-draining condition and (b) unstable flow for the air-confining condition. The arrows in Figure 7b indicate the position of developed fingers after the wetting front became unstable.

methods. According to (7), instability of the wetting front could be induced by the following factors or situations, including (1) a decrease in water pressure at the soil surface  $h_0$  or redistribution of water following infiltration ( $h_0$  becomes negative), (2) a decrease in the water-bubbling value of the porous media  $h_{wb}$  (owing to the occurrence of macropores or the presence of a fine-textured layer overlaying a coarse-textured layer), (3) infiltration into hydrophobic media (the value of  $h_{wb}$  is then negative), and (4) an increase in air pressure ahead of the wetting front  $h_{af}$ , a situation being considered in our study. *Diment and Watson* [1985] confirmed fingering as caused by factor 1. *Hill and Parlange* [1972], *Glass et al.* [1991], *Baker and Hillel* [1990], and *Selker et al.* [1992] focused on factor 2, whereas factor 3 was confirmed by *Hendrickx et al.* [1993] and *Ritsema et al.* [1993]. Although *White et al.* [1977] confirmed situation 4 with experiments in the Hele-Shaw cells, they were not successful with soils when the soil air was artificially compressed using a pumping system. From the time when *Peck* [1965] noticed “tongues” (fingered flow) in his air-confining soil columns, few if any systematic studies have been published on fingering due to natural air compression by infiltrating water.

Our 3-D experiments confirmed that when the instability criteria of (5) and (7) were satisfied the wetting front becomes unstable in the initially dry sand. Fingering occurred in all air-confining columns (Figures 2b, 4a, 4b, 4c, and 5) and also in the air-draining columns under the negative pressure source (Figure 3a). Finger development inside the 3-D column was indicated whenever the maximum wetting front  $Z_{\max}$  moved more quickly downward than the minimum front  $Z_{\min}$ . Results also indicate that when (5) and (7) are not satisfied the wetting fronts become stable. A sharp wetting front ( $Z_{\max} = Z_{\min}$ ) was maintained during the entire period of infiltration. Stable

flow occurred in all ponded air-draining columns (Figures 2a, 3b, and 3c). The effect of air entrapment on fingering was best visualized in our 2-D experiments, as shown in Figure 7. For the ponded air-draining infiltration experiment the wetting front (Figure 7a) was stable, consistent with the conditions that  $i_w > K_s$  and  $F > 0$ . A sharp wetting front remained present throughout the infiltration process. However, for the air-confining condition, when both instability criteria were satisfied ( $i_w < K_s$  at  $t = 2.5$  min and  $F < 0$  at  $t = 1$  min) owing to soil air compression, the wetting front became fingered (Figure 7b) after  $\sim 3$  min. Repeated experiments, also with large columns, have shown that the pattern of stable wetting for the air-draining condition and the pattern of unstable wetting for the air-confining condition were qualitatively reproducible. Random factors arising from the differences in sample packing and edge effects, and possibly other causes, affected only the quantitative features of the wetting fronts.

## 5. Summary and Conclusions

Infiltration of rainfall or irrigation water over a large surface area involves water inflow and air outflow, and possibly air compression. This dynamic process is difficult to observe quantitatively in the field. A laboratory experimental setup consisting of a transparent soil column, a tension-pressure infiltrometer, and an air flowmeter was developed and presented in this paper. Infiltration experiments under constant and time-varying positive and negative surface water heads, with and without air compression ahead of the wetting front, were carried out.

The infiltration rate under air-confining conditions generally fluctuated with time, rather than undergoing changes in a



three-stage process. When the air pressure ahead of the wetting front reached an air-breaking value, soil air escaped from the surface, leading to an immediate decrease in the air pressure and an increase in the infiltration rate. When the air pressure fell below a certain air-closing value, air escape stopped, the infiltration rate decreased again, and the air pressure increased. This cyclic process repeated itself during the entire infiltration period, with varying patterns depending on the stability of the surface water head. A minor decrease in surface water head was found to lead to an abrupt increase in infiltration rate. The air-breaking and the air-closing values were empirically related to the sum of the surface water head, the depth of the saturated top layer, and the air- and water-bubbling values of the material.

We confirmed experimentally in our 3-D and 2-D columns that air compression ahead of the wetting front will cause wetting front instability and flow fingering in a sandy medium. Although further study is needed to quantify the size and rates of fingered flow, our results indicate that the effects of the soil air phase cannot be neglected when modeling infiltration processes.

Macropore flow and fingering in unsaturated field soils are increasingly being considered as a rule rather than the exception [Flury *et al.*, 1994]. Fingered infiltration may lead to the accelerated transport of water and nonaqueous phase liquids toward the groundwater. Fingering also causes an uneven distribution of water and fertilizers in the crop root zone and increases their degree of leaching to the groundwater table. Thus further research on flow fingering due to air compression by infiltrating water, as well as other causes, is of importance for understanding underlying transport processes in the vadose zone.

**Acknowledgments.** This research project was funded by the Katholieke Universiteit Leuven. Comments made by several anonymous reviewers were greatly appreciated.

## References

- Adrian, D. D., and J. B. Franzini, Impedance to infiltration by pressure build-up ahead of the wetting front, *J. Geophys. Res.*, *71*, 5857–5862, 1966.
- Baker, R. S., and D. Hillel, Laboratory tests of a theory of fingering during infiltration into layered soils, *Soil Sci. Soc. Am. J.*, *54*, 20–30, 1990.
- Bodman, G. B., The variability of the permeability “constant” at low hydraulic gradients during saturated water flow in soils, *Soil Sci. Soc. Am. Proc.*, *2*, 45–53, 1937.
- Bouwer, H., Rapid field measurement of air entry value and hydraulic conductivity of soil as significant parameters in flow system analysis, *Water Resour. Res.*, *2*, 729–738, 1966.
- Chouke, R. L., P. van Meurs, and C. van der Poel, The instability of slow, immiscible, viscous liquid-liquid displacements in permeable media, *Trans. Am. Inst. Min. Metall. Pet. Eng.*, *216*, 188–194, 1959.
- Christiansen, J. E., Effects of entrapped air upon the permeability of soils, *Soil Sci.*, *58*, 355–366, 1944.
- Constantz, J., W. N. Herkelrath, and F. Murphy, Air encapsulation during infiltration, *Soil Sci. Soc. Am. J.*, *52*, 10–16, 1988.
- Corey, A. T., and R. H. Brooks, Drainage characteristics of soils, *Soil Sci. Soc. Am. Proc.*, *39*, 251–255, 1975.
- Diment, G. A., and K. K. Watson, Stability analysis of water movement in unsaturated porous materials, 3, Experimental studies, *Water Resour. Res.*, *21*, 979–984, 1985.
- Dixon, R. M., and D. R. Linden, Soil air pressure and water infiltration under border irrigation, *Soil Sci. Soc. Am. Proc.*, *36*, 948–953, 1972.
- Fallow, D. J., and D. E. Elrick, Field measurement of air entry and water entry soil water pressure heads, *Soil Sci. Soc. Am. J.*, *60*, 1036–1039, 1996.
- Fayer, M. J., and D. Hillel, Air encapsulation, I, Measurement in a field soil, *Soil Sci. Soc. Am. J.*, *50*, 568–572, 1986.
- Flury, M., H. Flüthler, W. A. Jury, and J. Leuenberger, Susceptibility of soils to preferential flow: A field study, *Water Resour. Res.*, *30*, 1945–1954, 1994.
- Glass, R. J., J.-Y. Parlange, and T. S. Steenhuis, Immiscible displacement in porous media: Stability analysis of three-dimensional, axisymmetric disturbances with application to gravity-driven wetting front instability, *Water Resour. Res.*, *27*, 1947–1956, 1991.
- Grismer, M. E., M. N. Orang, V. Clausnitzer, and K. Kinney, Effects of air compression and counterflow on infiltration into soils, *J. Irrig. Drain. Eng.*, *120*, 775–795, 1994.
- Hendrickx, J. M. H., L. W. Dekker, and O. H. Boersma, Unstable wetting fronts in water repellent field soils, *J. Environ. Qual.*, *22*, 109–118, 1993.
- Hill, D. E., and J.-Y. Parlange, Wetting front instability in layered soils, *Soil Sci. Soc. Am. Proc.*, *36*, 697–702, 1972.
- Hillel, D., and R. S. Baker, A descriptive theory of fingering during infiltration into layered soils, *Soil Sci.*, *146*, 51–56, 1988.
- Jalali-Farahani, H. R., D. F. Heermann, and H. R. Duke, Physics of surge irrigation, II, Relationship between soil physical and hydraulic parameters, *Trans. ASAE*, *36*(1), 37–44, 1993.
- Jarrett, A. R., and D. D. Fritton, Effect of entrapped soil air on infiltration, *Trans. ASAE*, *21*(5), 901–906, 1978.
- Klute, A., and C. Dirksen, Hydraulic conductivity and diffusivity: Laboratory methods, in *Methods of Soil Analysis*, edited by A. Klute, pp. 687–732, Am. Soc. of Agron., Madison, Wis., 1986.
- Latifi, H., S. N. Prasad, and O. J. Helweg, Air entrapment and water infiltration in two-layered soil column, *J. Irrig. Drain. Eng.*, *120*, 871–891, 1994.
- Linden, D. R., and R. M. Dixon, Infiltration and water table effects of soil air pressure under border irrigation, *Soil Sci. Soc. Am. J.*, *37*, 94–98, 1973.
- Luckner, L., M. T. van Genuchten, and D. R. Nielsen, A consistent set of parametric models for the two-phase flow of immiscible fluids in the subsurface, *Water Resour. Res.*, *25*, 2187–2193, 1989.
- McWhorter, D. B., Infiltration affected by flow of air, *Hydrol. Pap.* *49*, Colo. State Univ., Fort Collins, 1971.
- Morel-Seytoux, H. J., and J. A. Billica, A two-phase numerical model for prediction of infiltration: Application to a semi-infinite soil column, *Water Resour. Res.*, *21*, 607–615, 1985.
- Morel-Seytoux, H. J., and J. Khanji, Derivation of an equation of infiltration, *Water Resour. Res.*, *10*, 795–800, 1974.
- Parlange, J.-Y., and D. E. Hill, Theoretical analysis of wetting front instability in soils, *Soil Sci.*, *122*, 236–239, 1976.
- Peck, A. J., Moisture profile development and air compression during water uptake by air-confining porous bodies, 3, Vertical columns, *Soil Sci.*, *100*, 44–51, 1965.
- Perroux, K. M., and I. White, Designs for disc permeameters, *Soil Sci. Soc. Am. J.*, *52*, 1205–1215, 1988.
- Philip, J. R., Stability analysis of infiltration, *Soil Sci. Soc. Am. Proc.*, *39*, 1042–1049, 1975.
- Raats, P. A. C., Unstable wetting fronts in uniform and non-uniform soils, *Soil Sci. Soc. Am. Proc.*, *37*, 681–685, 1973.
- Ritsema, C. J., L. W. Dekker, J. M. H. Hendrickx, and W. Hamminga, Preferential flow mechanism in a water repellent sandy soil, *Water Resour. Res.*, *29*, 2183–2193, 1993.
- Saffman, P. G., and S. G. Taylor, The penetration of fluid into a porous medium or Hele-Shaw cell containing a more viscous liquid, *Proc. R. Soc. London, Ser. A*, *245*, 312–329, 1958.
- Sander, G. C., J.-Y. Parlange, and W. L. Hogarth, Air and water flow, II, Gravitational flow with an arbitrary flux boundary condition, *J. Hydrol.*, *99*, 225–234, 1988.
- Selker, J. S., T. S. Steenhuis, and J.-Y. Parlange, Wetting front instability in homogeneous sandy soils under continuous infiltration, *Soil Sci. Soc. Am. J.*, *56*, 1346–1350, 1992.
- Suhr, J. L., A. R. Jarrett, and J. R. Hoover, The effect of soil air entrapment on erosion, *Trans. ASAE*, *27*(1), 93–98, 1984.
- Touma, J., G. Vachaud, and J.-Y. Parlange, Air and water flow in a sealed, ponded vertical soil column: Experiment and model, *Soil Sci.*, *137*, 181–187, 1984.
- Vachaud, G., M. Vauclin, D. Khanji, and M. Wakil, Effects of air pressure on water flow in an unsaturated stratified vertical column of sand, *Water Resour. Res.*, *9*, 160–173, 1973.
- Vachaud, G., J. P. Gaudet, and V. Kuraz, Air and water flow during

- ponded infiltration in a vertical bounded column of soil, *J. Hydrol.*, 22, 89–108, 1974.
- van Genuchten, M. Th., A closed form equation for predicting the hydraulic conductivity of unsaturated soils, *Soil Sci. Soc. Am. J.*, 44, 892–898, 1980.
- White, I., P. M. Colombera, and J. R. Philip, Experimental studies of wetting front instability induced by gradual changes of pressure gradient and by heterogeneous porous media, *Soil Sci. Soc. Am. Proc.*, 41, 483–489, 1977.
- Wilson, L. G., and J. N. Luthin, Effects of air flow ahead of the wetting front on infiltration, *Soil Sci.*, 91, 137–143, 1963.
- Youngs, E. G., and A. J. Peck, Moisture profile development and air compression during water uptake by air-confining porous bodies, 1, Theoretical introduction, *Soil Sci.*, 98, 290–294, 1964.
- J. Feyen and Z. Wang, Institute for Land and Water Management, Katholieke Universiteit Leuven, Vital Decosterstraat 102, Leuven, Belgium 3000. (e-mail: zhi.wang@agr.kuleuven.ac.be)
- D. R. Nielsen, Department of Land, Air, and Water Resources, University of California, 1004 Pine Lane, Davis, CA 95616. (e-mail: drnielsen@ucdavis.edu)
- M. T. van Genuchten, U.S. Salinity Laboratory, USDA-ARS, 450 West Big Springs Road, Riverside, CA 92507-4617. (e-mail: titan@ucrvm.s)

(Received July 25, 1997; revised September 29, 1997; accepted September 30, 1997.)